RL-TR-92-314
In-House Report
December 1992

ENHANCED PHOTOREFRACTIVE EFFECTS IN BARIUM TITANATE

George A. Brost

APPROVED FOR PUBLIC RELEASE; DISTRIBUTION UNLIMITED.

This effort was funded totally by the Laboratory Director's fund.

Rome Laboratory
Air Force Materiel Command
Griffiss Air Force Base, New York

This report has been reviewed by the Rome Laboratory Public Affairs Office (PA) and is releasable to the National Technical Information Service (NTIS). At NTIS it will be releasable to the general public, including foreign nations.

RL-TR-92-314 has been reviewed and is approved for publication.

APPROVED: James W. Cusack

JAMES W. CUSACK, Chief
Photonics & Optics Division
Surveillance & Photonics Directorate

FOR THE COMMANDER:

JAMES W. YOUNGBERG, LtCol, USAF
Deputy Director
Surveillance & Photonics Directorate

If your address has changed or if you wish to be removed from the Rome Laboratory mailing list, or if the addressee is no longer employed by your organization, please notify RL (OCPA) Griffiss AFB NY 13441-5700. This will assist us in maintaining a current mailing list.

Do not return copies of this report unless contractual obligations or notices on a specific document require that it be returned.

REPORT DOCUMENTATION PAGE

Form Approved
OMB No. 0704-0188

1. AGENCY USE ONLY (Leave Blank)	2. REPORT DATE	3. REPORT TYPE AND DATES COVERED
	December 1992	In-House Oct 89 - Sep 92

4. TITLE AND SUBTITLE
ENHANCED PHOTOREFRACTIVE EFFECTS IN BARIUM TITANATE

5. FUNDING NUMBERS
PE - 61101F
PR - LDFP
TA - 10
WU - H0

6. AUTHOR(S)
George A. Brost

7. PERFORMING ORGANIZATION NAME(S) AND ADDRESS(ES)
Rome Laboratory (OCPA)
25 Electronic Parkway
Griffiss AFB NY 13441-4515

8. PERFORMING ORGANIZATION REPORT NUMBER
RL-TR-92-314

9. SPONSORING/MONITORING AGENCY NAME(S) AND ADDRESS(ES)
Rome Laboratory (OCPA)
25 Electronic Parkway
Griffiss AFB NY 13441-4515

10. SPONSORING/MONITORING AGENCY REPORT NUMBER

11. SUPPLEMENTARY NOTES
Rome Laboratory Project Engineer: George A. Brost/OCPA (315) 330-7669

12a. DISTRIBUTION/AVAILABILITY STATEMENT
Approved for public release; distribution unlimited.

12b. DISTRIBUTION CODE

13. ABSTRACT (Maximum 200 words)

This report documents investigations of characteristics of secondary centers (shallow traps) in $BaTiO_3$, and the possible utilization of these traps for enhanced photorefractive effects at infrared wavelengths. Secondary centers were characterized by photo-induced absorption and two-beam coupling experiments. Two species were identified, with concentrations of approximately 1.5×10^{17} cm $^{-3}$ and 2×10^{16} cm $^{-3}$. The effect of secondary centers on the sublinear intensity dependence and temperature dependent photorefractive effects were also examined. No enhancements of photorefractive effects were also examined. No enhancements of photorefractive effects from induced population of secondary centers by external pumping were observed.

14. SUBJECT TERMS	15. NUMBER OF PAGES
photorefraction, barium titanate	56
	16. PRICE CODE

17. SECURITY CLASSIFICATION OF REPORT	18. SECURITY CLASSIFICATION OF THIS PAGE	19. SECURITY CLASSIFICATION OF ABSTRACT	20. LIMITATION OF ABSTRACT
UNCLASSIFIED	UNCLASSIFIED	UNCLASSIFIED	U/L

CONTENTS

I. INTRODUCTION

Photorefractive nonlinear effects such as two-wave mixing and phase conjugation can be utilized for a variety of image and signal processing applications. The useful spectral range of those crystals which offer high gain is limited to visible wavelengths. Although photorefractive effects have been observed in the near infrared in $BaTiO_3$ (barium titanate), the sensitivity has been too low for practical application at these wavelengths.

A possible technique for enhancing the photorefractive effect in $BaTiO_3$ at laser diode wavelengths was based on the concept of secondary photorefractive centers introduced by Brost *et al.*[1]. New (unpublished) data had indicated that the population of secondary centers would increase the absorption coefficient at 800 nm. The concept was to populate these centers in a manner which could increase the sensitivity.

This report documents efforts to better understand the characteristics of the secondary centers and to explore an enhancement technique based on their presence in $BaTiO_3$. In section II a background on photorefraction and secondary centers is given. Section III describes photo-induced absorption and two-beam coupling experiments designed to yield information on the secondary centers. In section IV photorefractive enhancement studies, theoretical and experimental, are described. Although the desired enhancements were not realized, these efforts have provided useful information about the secondary centers. In addition the theoretical development has applications in other

areas. In section V additional photorefractive characteristics of sublinear intensity dependent rise time and temperature dependent photorefractive effects resulting from the presence of secondary centers are discussed.

II. BACKGROUND

The physical process involved in the photorefractive effect is a light induced redistribution of charges among traps. The resulting space charge field then modulates the refractive index through the linear electro-optic effect. Based on the simple band transport model of a single set of recombination centers Kuhktarev *et al.*[2] derived solutions for formation of the photorefractive grating. These solutions have provided fairly good agreement with many experiments. In an effort to account for intensity dependent absorption and photorefractive effects in $BaTiO_3$ Brost *et al.*[1] introduced the secondary center model. Secondary photorefractive centers were traps which were highly thermalized at room temperature but became populated under the illumination by visible light. This model was based on one set of secondary centers. Brost *et al.*[1] considered only absorption effects at 514 nm. In this effort, the secondary center model for $BaTiO_3$ was extended to two species of secondary centers, as suggested by the photo-induced absorption data. This model is shown schematically in Figure 1. The concept for enhancing the photorefractive effect in $BaTiO_3$ which utilizes the secondary centers is shown in Figure 2. The concept is to illuminate the

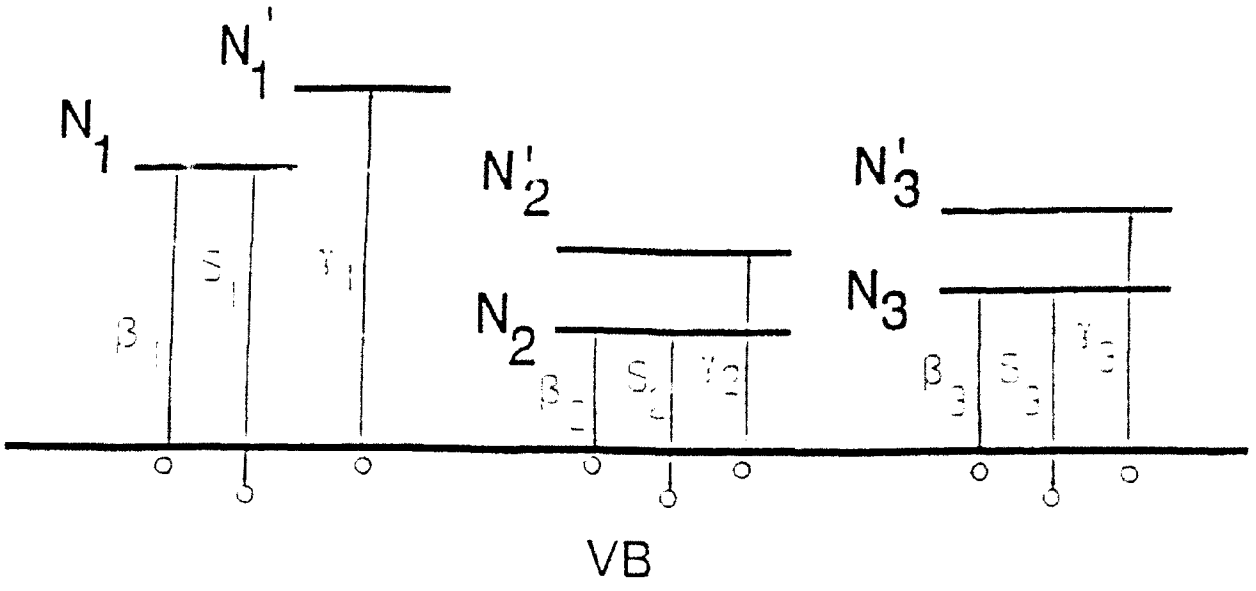

Figure 1. Schematic diagram of secondary center model for $BaTiO_3$.

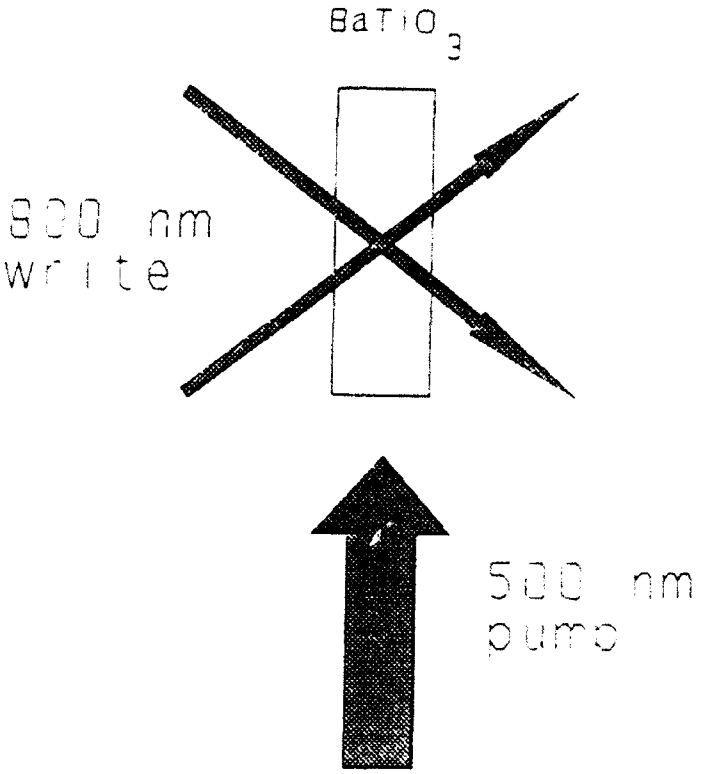

Figure 2. Sechmatic diagram of concept for enhancement of photorefractive effects in $BaTiO_3$ through external pumping.

crystal with pump beam of visible wavelength while writing the photorefractive grating with a cw laser at a near infrared wavelength. It was hoped that the population of the secondary centers by the pump beam could result in an enhancement through an increased sensitivity associated with the increased absorption in the near infrared.

The response of the photorefractive material to a spatially modulated light intensity pattern is well described by a set of nonlinear differential equations. The relevant equations for the secondary center shown in Figure 1 are

$$dN_1/dt = -(S_{11}I_1 + S_{12}I_2 + \beta_1)N_1 + \gamma_1(N_{1T} - N_1)N_h \quad (1)$$

$$dN_2/dt = -(S_{21}I_1 + S_{22}I_2 + \beta_2)N_2 + \gamma_2(N_{2T} - N_2)N_h \quad (2)$$

$$dN_3/dt = -(S_{31}I_1 + S_{32}I_2 + \beta_3)N_3 + \gamma_3(N_{3T} - N_3)N_h \quad (3)$$

$$dN_h/dt = -dN_1/dt - dN_2/dt - dN_3/dt \quad (4)$$

$$\partial N_h/dt = dN_h/dt - \nabla\cdot j_h \quad (5)$$

$$j_h = \mu_h N_h E - D\nabla N_h, \quad (6)$$

$$\nabla\cdot E = \rho/\epsilon\epsilon_o, \quad (7)$$

where N_{1T} is the total number density of photorefractive centers, N_{2T} and N_{3T} are the total number densities of the secondary centers, N_i is the number density of unionized charge donors, N_h is the number density of free carriers (these equations are written for positively charged free carriers), j_h is the free carrier current density, I_1 and I_2 are the light intensities of two different wavelengths, $S_{i1,2}$ are the photon-

absorption cross sections for light of wavelengths 1 and 2, γ_i is the recombination coefficient, β_1 is the thermal ionization rate, μ_h is the carrier mobility, *D is the diffusion coefficient given* by $D = \mu_h k_B T/q$, **E** is the electric field, ϵ is the dielectric constant, ϵ_o is the permittivity of free space, ρ is the charge density. These equations are subject to the constraint of charge conservation

$$N_1 + N_2 + N_3 + N_h - N_o = 0, \qquad (8)$$

where $N_o = N_{1d} + N_{2d} + N_{3d} + N_{hd} + N_{hd}$, and the N_{id} are the initial dark concentration levels before the light was turned on. The two beam coupling gain coefficient is then related to the photorefractive space charge field through

$$\Gamma = n^3 \pi r_{eff} \mathrm{Im}(E_1) \qquad (9)$$

where n is the refractive index, r_{eff} is the effective electro-optic coefficient and E_1 is the fundamental component of the space charge field.

For photorefractive effects, the light intensity pattern is assumed to be spatially periodic and of the following form:

$$I(x,t) = I_o(t)\{1 + m\sin[Kx]\}, \qquad (10)$$

where I_o is the total intensity, m is the modulation index, K is the grating wave number. For two vertically polarized input

waves of intensities I_S and I_R, $m = 2\beta^{1/2}/(\beta+1)$, where $\beta = I_R/I_S$.

Examination of equations (1-10) indicate that there are eighteen input parameters, eight of which are directly related to the secondary centers. Most of these parameters associated with the secondary centers were unknown. Consequently experiments were conducted to improve the understanding of the secondary centers.

III. SECONDARY CENTER CHARACTERIZATION

This section describes results of experiments designed to further characterize the secondary centers in $BaTiO_3$. By analyzing many separate, but related experiments and improved picture of the secondary centers could be obtained. These included photo-induced absorption and two-beam coupling experiments.

Photo-induced absorption

A important characteristic of the secondary centers is the presence of photo-induced absorption. Motes and Kim [3] first reported the existence of what was called intensity dependent absorption. In their experiments, the absorption coefficient of an argon ion laser was found to depend on its intensity. Brost *et al.*[1] later explained this absorption in terms of the secondary center model. In this report, the intensity dependent experiments were extended to measure the photo-induced absorption spectrum.

A schematic diagram of the experiment is shown in Figure 3. Photo-induced absorption was generated in the barium titanate crystal by illumination with the 514 nm line of an argon-ion

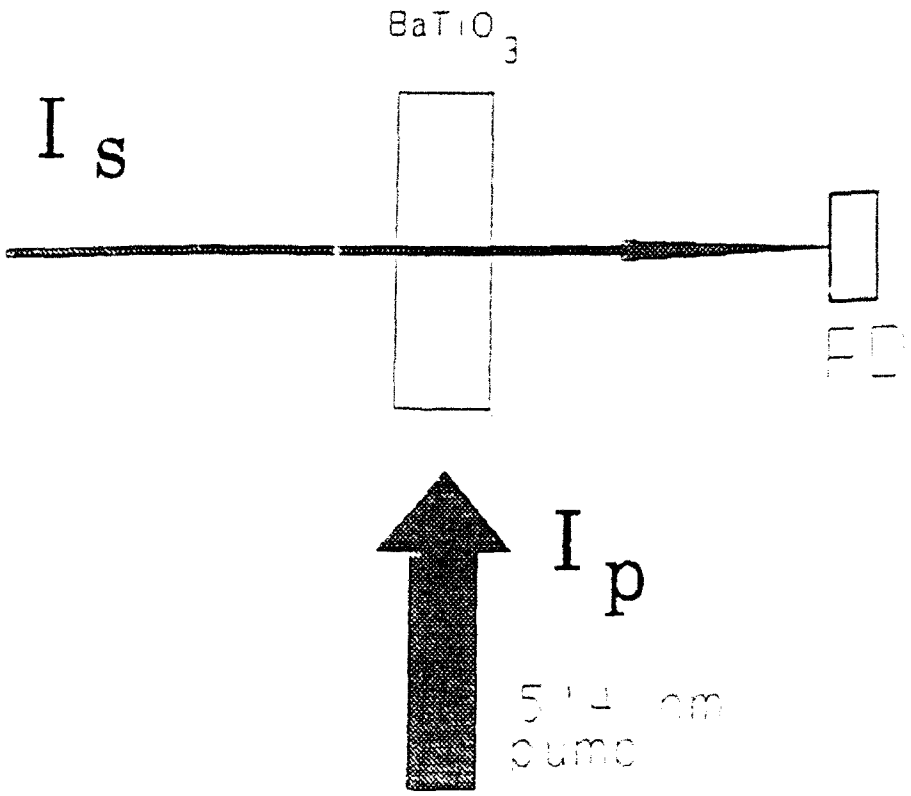

Figure 3. Schematic diagram of experimental arrangement for measurement of photo-induced absorption characteristics.

laser. The transmitted power of a weak signal beam (I_S) was monitored by a large area photodiode. The signal beam was obtained from a monochromator illuminator consisting of a tungsten halogen lamp and a grating monochromator. It was focused to approximately 1.5 mm diameter in the barium titanate crystal. The intensity of the signal beam varied between 3 and 100 W/cm^2, depending upon wavelength and polarization. The pump beam was expanded to fully illuminate the face of the crystal, which was 5 x 5 mm^2. Care was taken to minimize scattered light from the pump beam reaching the photodiode by use of filters and beam stops.

The magnitude of I_S was reduced in the presence of the argon laser pump beam (I_p) due to the photo-induced absorption. The photo-induced component of the absorption coefficient, α_I, was determined using the relation

$$\frac{I_S \text{ (with } I_p \text{ on)}}{I_S \text{ (with } I_p \text{ off)}} = \exp(-\alpha_I d), \qquad (11)$$

where d is the interaction length. A typical spectrum of the induced steady-state absorption is shown in Figure 4. The induced absorption spectrum did not depend on the polarization of the pump light. An anisotropy with respect to the polarization of the signal light was observed. The magnitude of the induced absorption for extraordinary polarized light was about 35% less than that for ordinary polarization. A germanium detector was used to check the spectrum between 1.0 and 1.8 m. No photo-induced absorption peaks were found in that region.

The temporal (rise and decay) characteristics of the induced

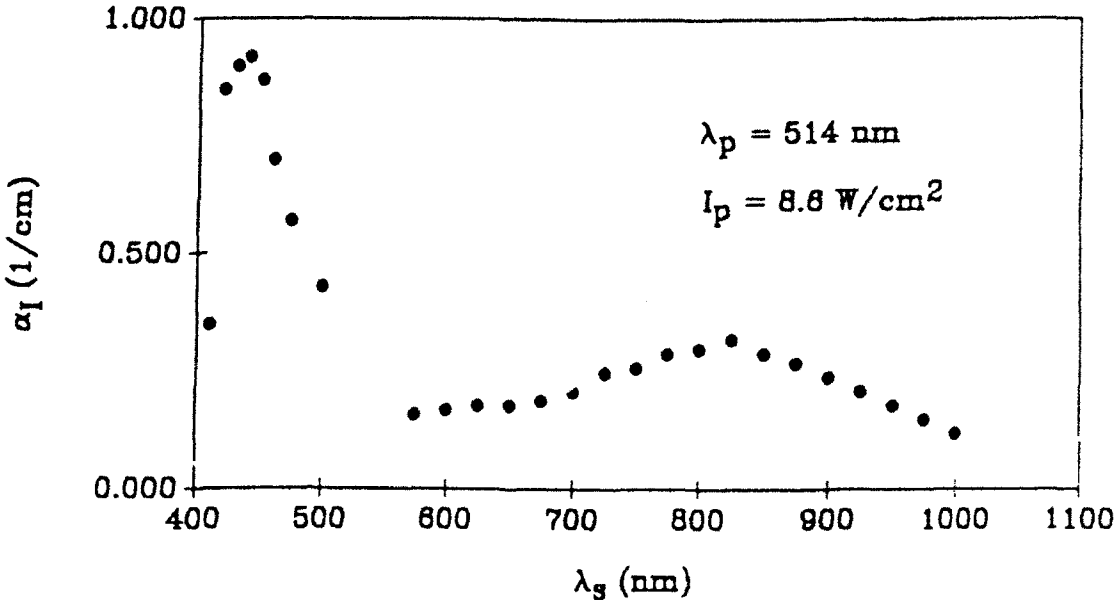

Figure 4. Steady state photo-induced absorption spectrum in $BaTiO_3$.

absorption were measured by turning the pump beam on for a time period sufficient to establish steady-state conditions while monitoring the signal beam transmission, as shown in Figures 5 and 6. The rise time for the absorption to reach steady-state depended upon the pump intensity, and was typically about an order of magnitude faster than the photorefractive grating formation time. The dark decay characteristics depended upon the signal beam wavelength. At 440 nm the induced absorption was characterized by a fast decay rate of approximately 60 ms time constant. At 800 nm two distinct decay rates were apparent: a fast decay similar to that at 440 nm, and a slow component, with a time constant of about 6 s. The spectrum could thus be separated into two components, "fast" and "slow", as shown in Figure 7. Here the slow decay spectrum was defined as the absorption remaining 2 seconds after the pump beam was turned off, and the fast decay was the remainder of the steady state absorption. The broad infrared steady-state absorption peak could then be separated into two absorption peaks at 775 and 820 nm.

The relative magnitudes of the "slow" and "fast" decay components of the induced absorption depended upon the intensity of the pump beam. This is seen in the data shown in Figure 8 for a 800 nm wavelength signal beam and a pump intensity of 4.3 mW/cm^2. Only the "slow" absorption component was induced with this low pump intensity. The magnitude of the slow component saturated at a pump intensity of about 10 mW/cm^2. The fast decay component required higher laser intensities and was observed only for pump intensities above 30 mW/cm^2, and saturated at about 10

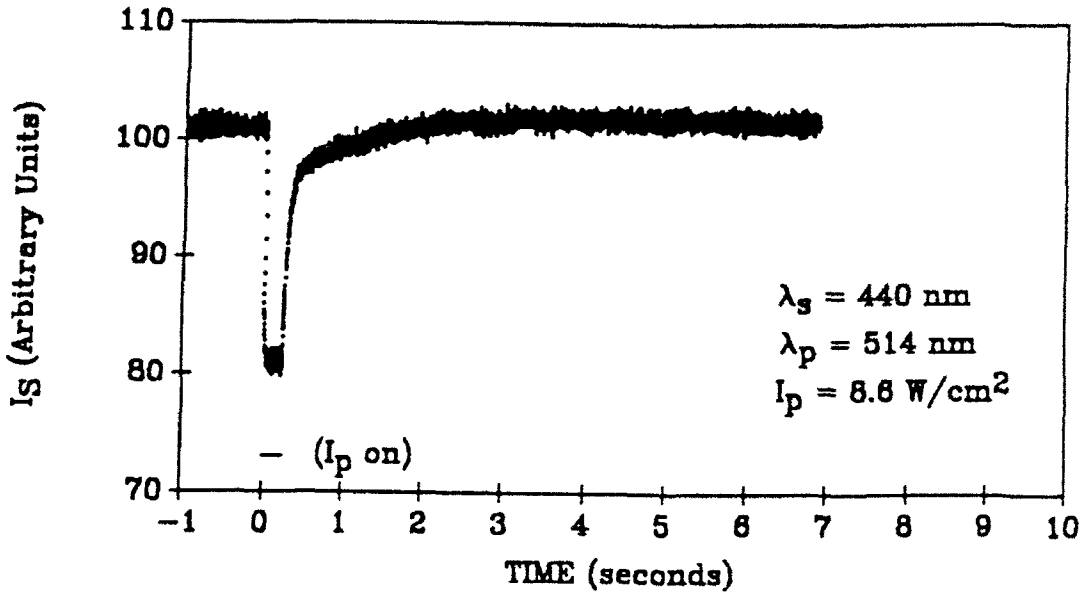

Figure 5. Signal beam transmission (I_S) versus time for 440 nm wavelength sigal beam.

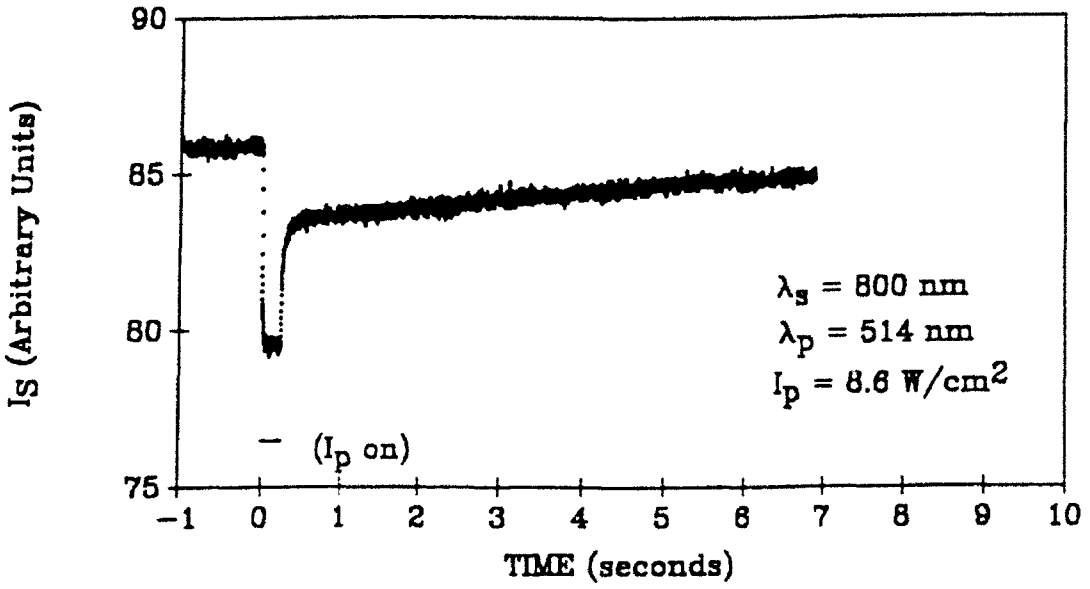

Figure 6. Signal beam transmission (I_S) versus time for 800 nm wavelength signal.

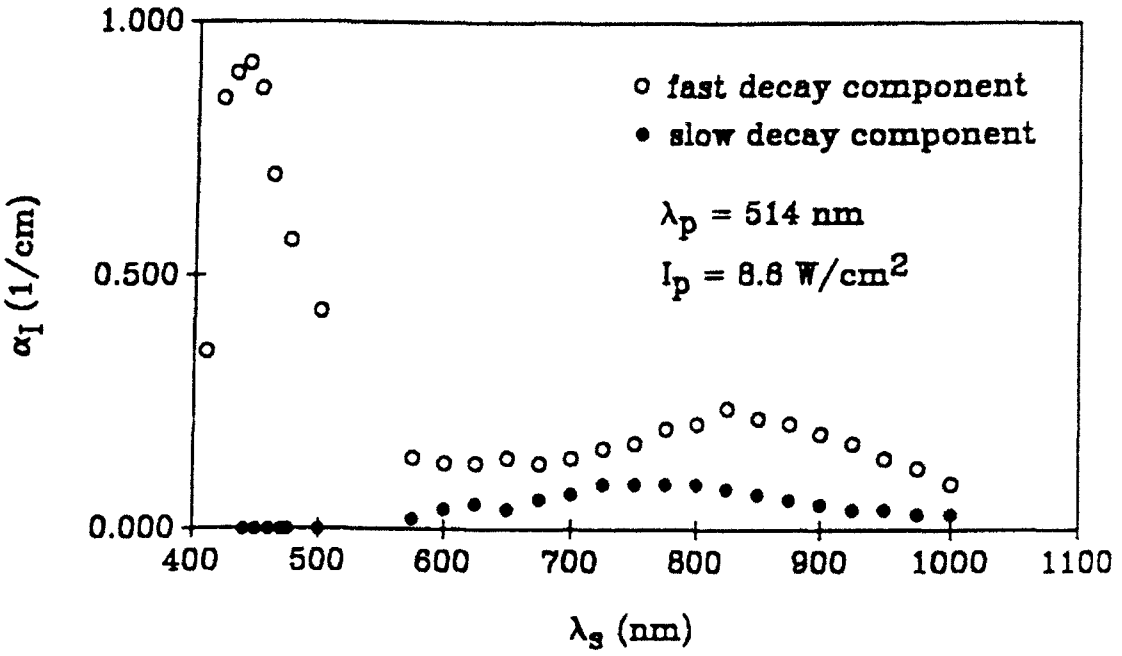

Figure 7. Time-resolved photo-induced absorption spectrum in $BaTiO_3$.

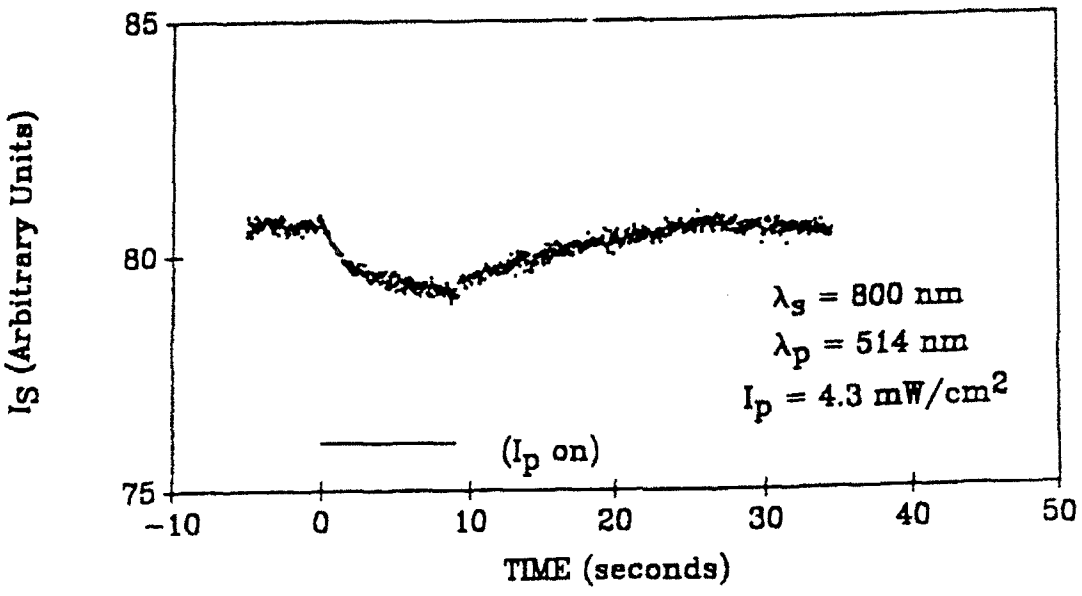

Figure 8. Signal beam transmission (I_S) versus time for 800 nm wavelength signal with low intensity pump beam.

W/cm^2. The intensity dependence is shown in Figure 9.

This photo-induced absorption data indicates that there are two dominant secondary photorefractive centers. The magnitude of the photo induced absorption coefficient at saturation provides useful information about the secondary centers through the relation

$$\alpha_i = S_i N_{iT}. \tag{12}$$

Temperature dependent measurements of the photo-induced absorption were also preformed. The goal of these experiments was to measure the thermal activation energy of the secondary centers by measuring the temperature dependence of the decay rate of the photo-induced absorption. For these experiments the $BaTiO_3$ crystal was mounted inside a glass cell containing silicon oil. The cell was heated with a hot plate and the temperature was monitored with a thermo-couple probe. Based on the photo-induced absorption spectrum measurements, it was possible to selectively probe the fast and slow decay components of the photo-induced absorption corresponding to N_2 and N_3, by the choice of signal wavelength. A 457 nm line from an argon ion laser was used as a probe of the fast decay component. For the slow decay component a 750 nm diode laser was used.

The magnitude of the photo-induced absorption decreased with increasing temperature. This is demonstrated in Figure 10 where the temperature dependence of the photo-induced absorption coefficient is plotted for a pump intensity of 10 W/cm^2. This decrease in absorption is attributed to the increased thermal ionization rate with increasing temperature.

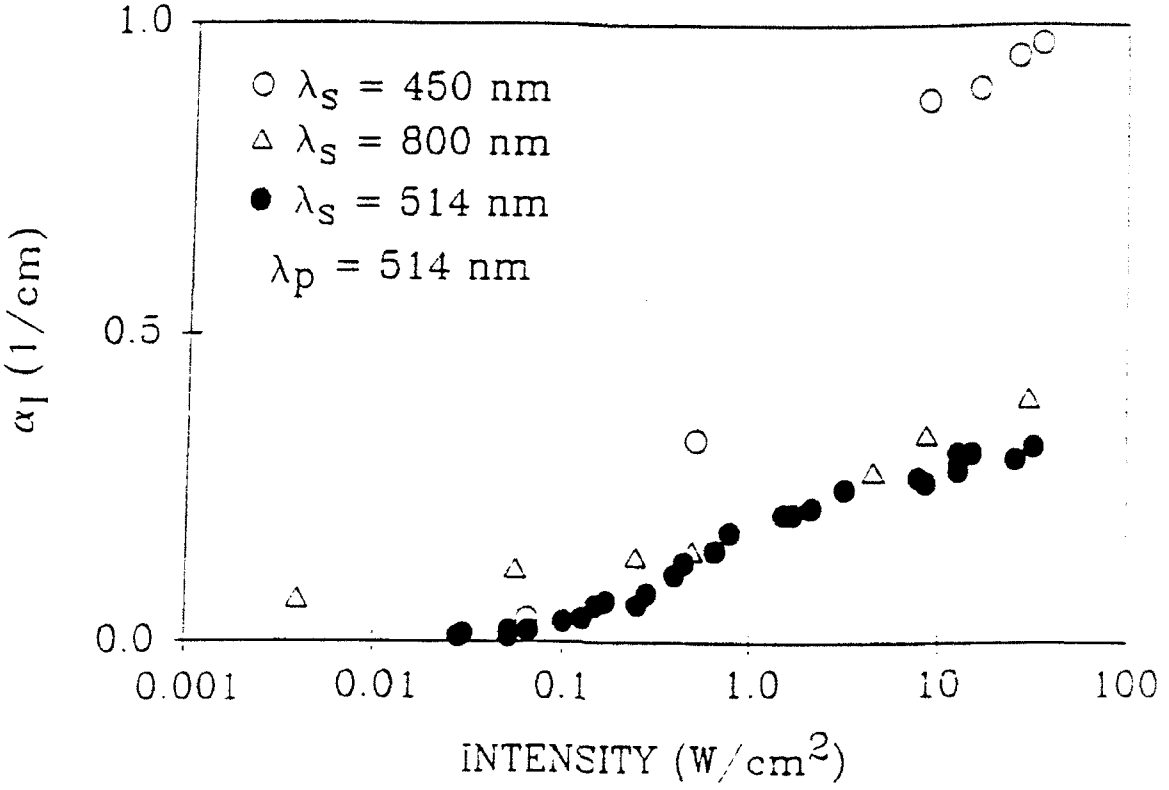

Figure 9. Intensity dependence of photo-induces absorption at various signal wavelengths for a 514 nm pump beam.

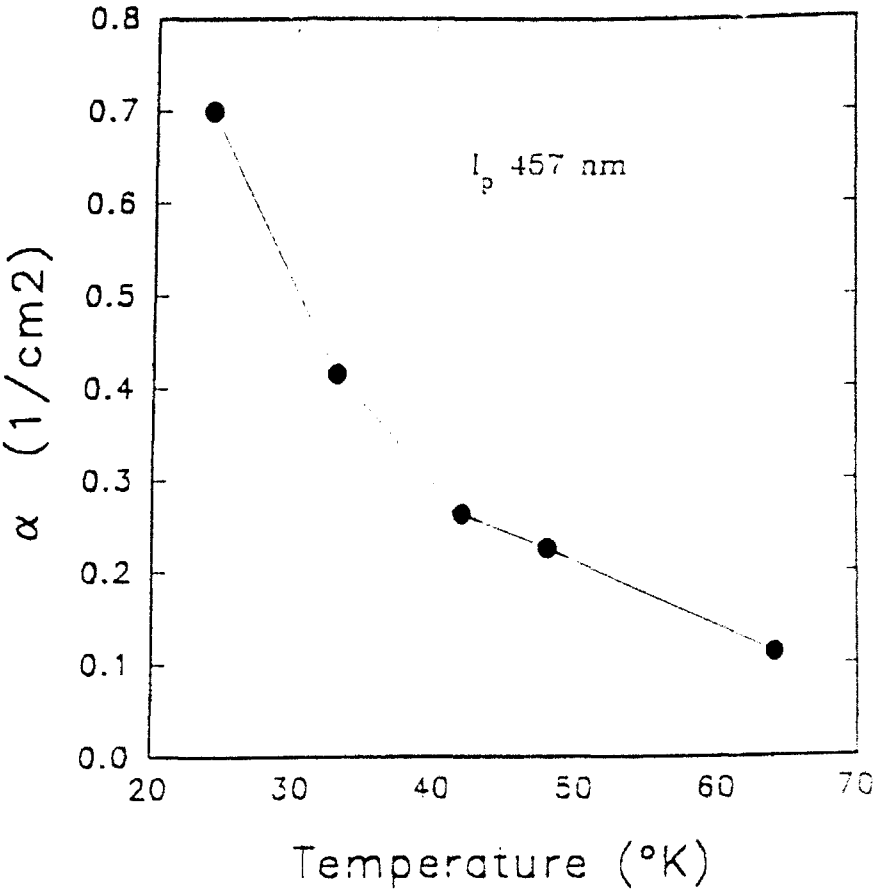

Figure 10. Temperature dependece of the photo-induced absorption coefficient at 457 nm for a 10 W/cm^2 pump intensity at 514 nm.

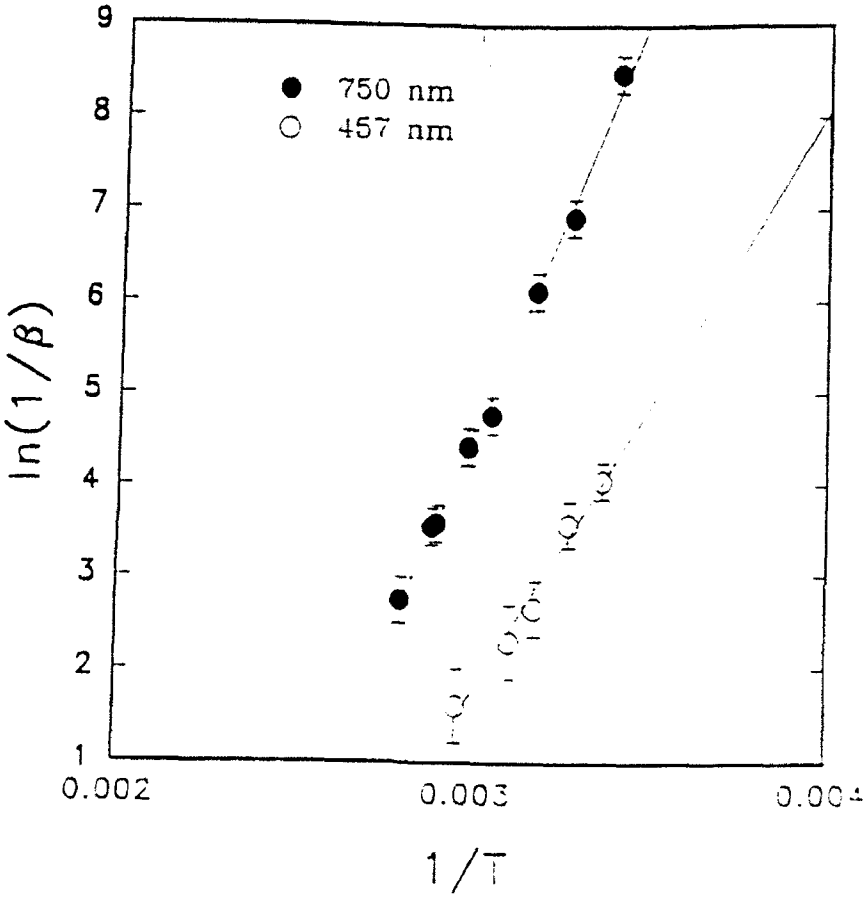

Figure 11. Photo-induced absorption decay time as function of temperature.

The results of the thermal decay experiments are shown in Figure 11. Here the thermal decay time is plotted on an Ahrenius plot as the natural log of 1/ß versus 1/T. The linear relationship on this plot indicates that a thermal activation energy in the form of equation 11. From this data the thermal activation energies for the fast and slow decay components were determined to be 0.5 and 0.8 eV, respectively.

Two Beam Coupling Experiments

Additional information about the secondary centers can be obtained from two beam coupling experiments. An estimate of the total concentrations N_{2T} and N_{3T} can be obtained from the intensity-dependent two beam coupling data. According to the band transport model of photorefraction the maximum two-wave mixing gain coefficient will occur at a grating period that is equal to the Debye screening length L_S, which is given by

$$L_S^2 = \epsilon\epsilon_o k_B T/q^2 N_E. \qquad (13)$$

The effective empty trap concentration N_E can then be determined from a photorefractive measurement of L_S. As shown by Brost et al. [1], the intensity dependent population of the secondary centers results in an intensity-dependent effective empty trap concentration. The difference in the high and low intensity values of N_E is approximately equal to the secondary center concentration. The intensity-dependent two-beam coupling data for a wavelength of 514 nm reported by Brost et al. [1] is shown in Figure 12. This data indicated that the total secondary

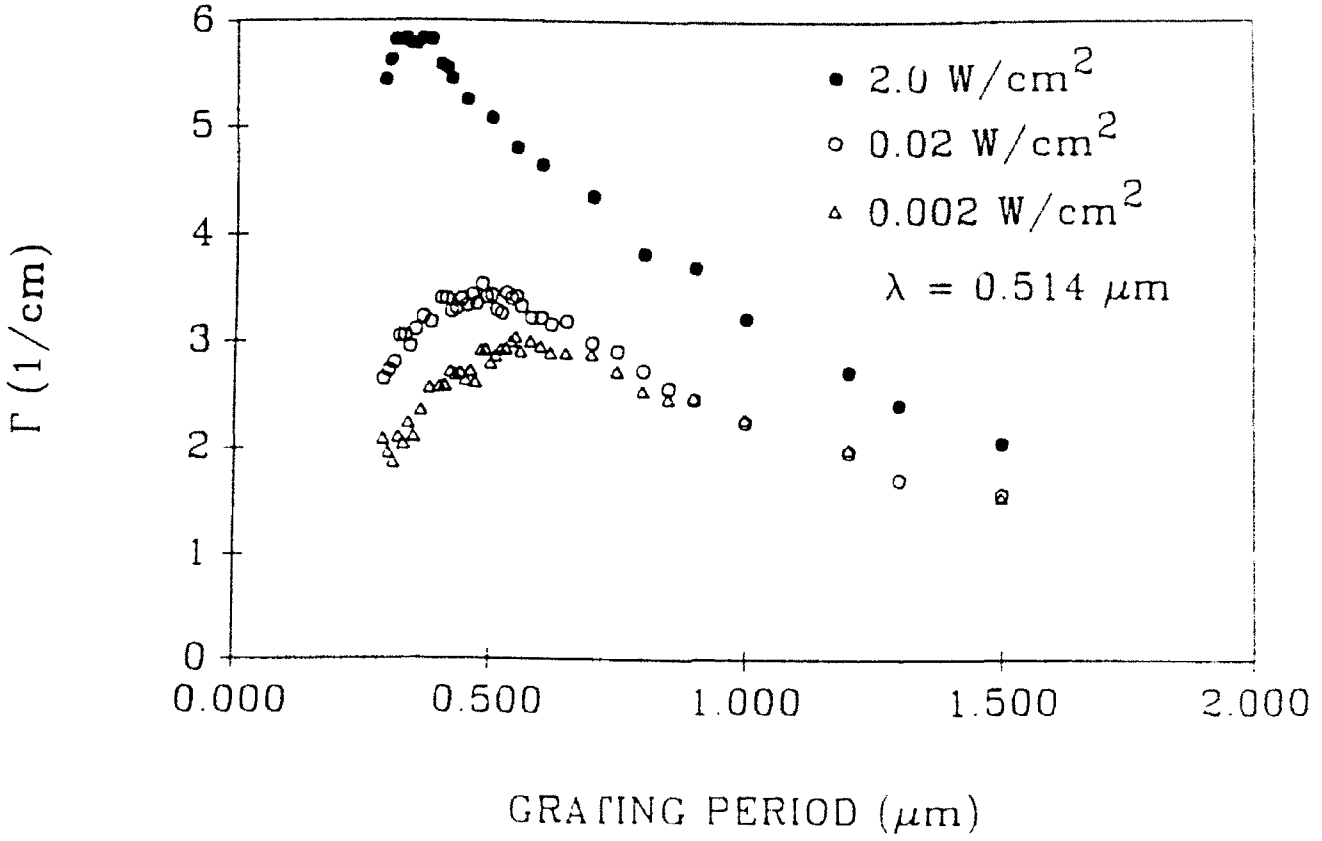

Figure 12. Intensity dependent two beam coupling gain versus grating period for 514 nm wavelength.

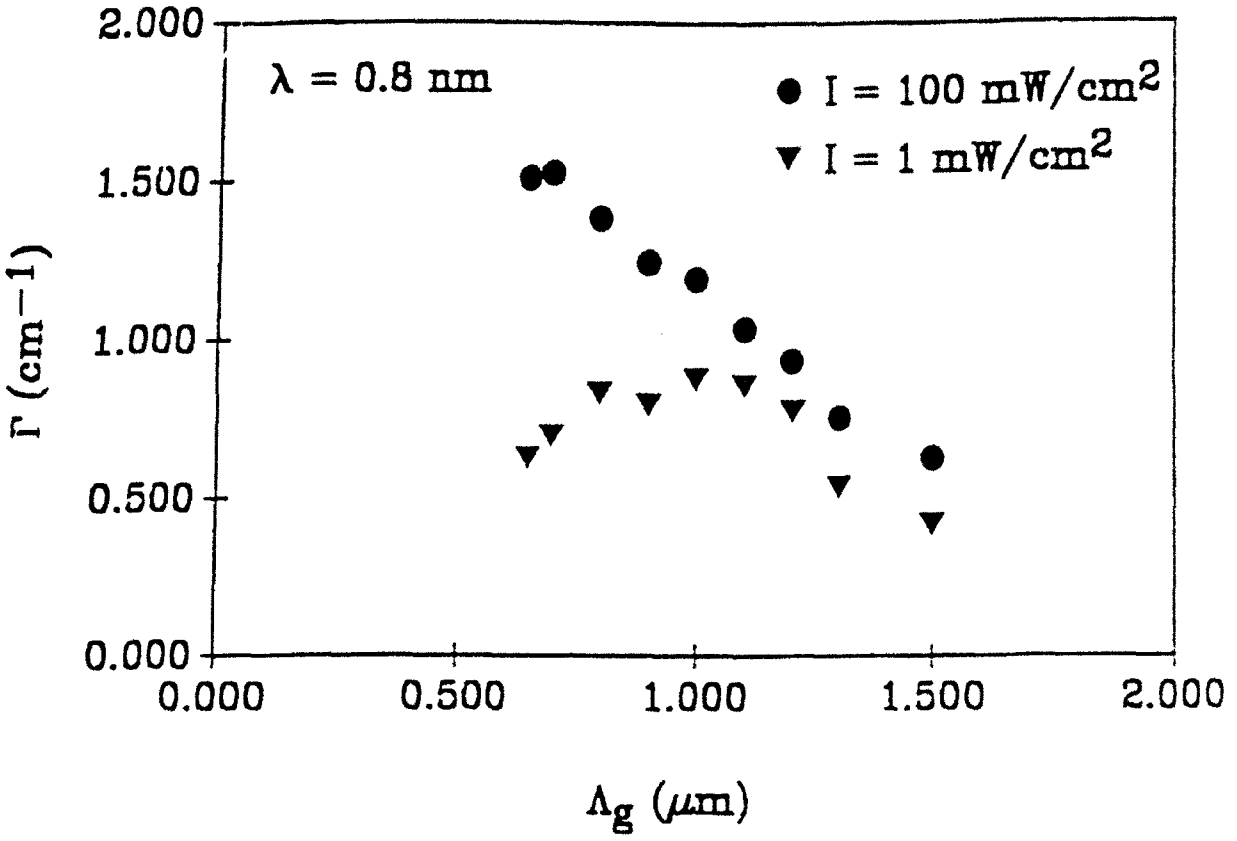

Figure 13. Intensity dependent two beam coupling gain versus grating period for 800 nm wavelength.

center concentration was approximately 1.5 x 10^{17} cm^{-3}. Two-beam coupling data taken at 800 nm wavelength is shown in Figure 13. These results indicate that at infrared wavelengths at very low intensities (1 mW/cm^2) secondary centers do not contribute to the photorefractive effect, and N_E is approximately $9x10^{15}$ cm^{-3}. But at somewhat higher intensities (100 mW/cm^2) the secondary centers (corresponding to N_3) do contribute to the photorefractive effect. From this data we can estimate that the N_3 secondary center concentration is about $2.5x10^{16}$ cm^{-3}. It is also apparent that at these moderate intensity levels external pumping of the secondary centers will not result in strong enhancements as the secondary centers are already contributing to the photorefractive effect.

IV. PHOTOREFRACTIVE ENHANCEMENTS

The photorefractive enhancements from utilization of the secondary centers were explored theoretically and experimentally. Although the desired enhancements were not realized, these efforts were are described below.

Theory

The equations (1-10) were studied theoretically to try to determine the optimum conditions for photorefractive enhancement. Two approaches were developed to solve nonlinearly coupled equations describing the photorefractive effect. The first

approach based on the small m approximation was appropriate for conditions of cw illumination. To study the effects of pulsed illumination, a second technique was developed based on a finite difference technique.

In the first approach the small modulation approximation was made in which only the first order terms are kept in the solution. Solution of the material equations proceeded by setting N_1, N_2, N_3, N_h, and E to the form $X = X_0 + X_1$ and solving for the lowest Fourier component in the quasi-steady approximation. The X_0 quantities are assumed to be independent of space and time, and used as input parameters for the equations involving X_1. This approach linearized the equations. The rate equations were solved numerically to determine the zeroth order terms. After eliminating the current, a set of linear equations in five variables remained. Analytical expressions were intractable, and consequently the solutions were obtained numerically. This approach was appropriate only for continuous illumination. Photorefractive space charge fields were calculated for the conditions in which the laser write beams (corresponding to I_1) were assumed to be at 800 nm, while the crystal was illuminated with a pump argon beam at 514 nm. Parameters for the secondary centers were based on measurements reported elsewhere in this report. A range of laser intensities of both the write beams and the pump beams were tried. In all cases, no conditions of enhancement could be found. The grating erasing effect of the argon pump beam was always greater than any enhancement effects due to the population of the secondary centers.

In order to determine the characteristics of the space-charge field under conditions of pulsed illumination of the pump beam a finite difference scheme was developed to model the photorefractive grating formations. Unfortunately, this approach was very computer intensive. The nonlinearly coupled material equations were very unstable, requiring a small time step. It turned out to be impractical to use this approach model interactions in $BaTiO_3$, due to the extensive cpu time required. However, this approach has been successfully used to model photorefractive grating formations in other crystals.

In the second approach, the microscopic space-charge field was calculated under the assumptions that the spatial symmetry of the grating formation was one dimensional and periodic in the grating vector direction. With these assumptions, it was only necessary to calculate the charge redistribution over one grating period of length, which was divided into N cells. The electric field, and free carrier, carrier current, and charge densities were determined for each cell. The current was allowed to flow for a time period δt and the change in the free carrier concentration was determined by the continuity equation. The distribution of charge among free carriers and traps was then recalculated and the other quantities updated.

The distribution of charges among the traps and free carrier concentrations in each cell were determined from the rate Eqs (1-3) carriers in the ith cell due to the nonuniform current flow. Since ΔN_{hi} changes at each time step, the constraint given by Eq. (8) also varies at each time iteration. Two techniques

were used to solve the rate equations. The first technique was based on the quasi static approximation in which the time for establishing free carrier equilibrium was assumed to be much faster than the grating formation time. In this approximation the rate equations were solved for the steady state solution at each time step. This approach was not cpu intensive and worked well for cw illumination, but could not work with pulsed illumination. For pulsed illumination, a fourth order Runge Kutta technique was used to integrate the rate equations.

The free carrier current was then determined for each cell from Eq. (4). The photoinduced space charge field could be determined by combining the one dimensional continuity equation with Poisson's equation to give

$$E_{SC}(x,t) = -q/\epsilon\epsilon_o \int_0^t j_h(x,t)\, dt + G(t), \qquad (14)$$

where G(t) is determined from the boundary condition of the constraint of a constant applied voltage given by

$$-\int_0^L E(x,t)dx = V, \qquad (15)$$

where $E(x,t) = E_{SC}(x,t) + E_A(t) = E_{SC}(x,t) - V(t)/L$ is the total electrostatic field and L is the crystal length. With the assumption of periodicity this means that

$$\int_{x'}^{x'+\Lambda} E_{SC}(x,t)dx = 0. \qquad (16)$$

The space charge field was determined by applying Eqs. (14-16).

The one dimensional continuity equation was used in the following form to determine the change in the free carrier concentration in the ith cell:

$$\Delta N_{hi} = -(\nabla \cdot j_{hi})\delta t. \qquad (17)$$

The results from Eq. (17) were used to update the charge conservation constraint given by Eq. (8) in the solution of the rate equations on the next iteration.

These calculations provided a temporal evolution of the space charge field as well as other quantities such as free carrier and charge densities. For stability, the time step at each iteration was required to be less than the free carrier lifetime and characteristic transport times. For parameters appropriate to $BaTiO_3$, this meant time steps of less than 1 nsec even for cw illumination. When considering that grating formation times can be many seconds, this approach of integrating the rate equations required too much cpu time to be of practical use. Attempts were made to combine the quasi-static approach with the Runge Kutta integration to study the effects of pulsed illumination from the pump beam while writing the grating with cw beams, and thereby reduce the cpu time. Unfortunately these attempts were unsuccessful.

Experiment

Experiments were conducted to test out the enhancement concept depicted in Figure 2. In these experiments a 800 nm line from a Ti:saphire laser was used for the two beam coupling. The signal beam I_1 was monitored for enhancements in either the speed of the grating formation or the magnitude of the two-beam coupling gain. Either a doubled Nd:YAG laser or the 514 nm line from an argon-ion laser was used as the pump beam.

In the first set of experiments a cw pump beam was used. Intensity levels on the order of a few mW/cm^2 were used. As expected from the theoretical modeling no enhancements were observed. The presence of a cw pump beam had the effect of simply increasing the dark current and thereby lowering the gain. The erasure due to the pump beam dominated any enhancements effects that might be present.

The next approach to enhancement was to pulse the pump beam. It was anticipated that if the secondary centers could be populated with a short pulse of green light then the erasure effects would be minimized. It was known from the photo-induced absorption experiments that the time required to populate the secondary centers was much shorter than the time required to write the grating. A number of pulse illumination configurations were tested. A mechanical shutter was tested for illuminations > greater than 1 msec. An acousto-optic bragg cell was used as a shutter for illuminations down to a few microseconds. These pulsed illumination experiments were tested for a variety of repetition rates and illumination intensities. Although the

erasure effects were much less noticeable than with the cw illumination, no enhancemets were observed.

It was thought that if the pulsed illuminations could be made sufficiently short then there would be little or no erasure from the free carriers. The free carrier lifetime in $BaTiO_3$ is thought to be on the order of 1 nsec. The diffusion lengths of a free carrier in $BaTiO_3$ is approximately 0.02 μm, which is much less than the typical grating period of 0.5 μm. Consequently, for very short pulse illuminations the free carriers would be trapped before traveling the distance of 1/2 grating period needed to erase the grating. To test the enhancement with short pulses a Q-switched Nd:YAG laser was used. The pulse widths were approximately 5 nsec. Pump repetition rates ranged from 0.5 to 10 Hz. Fluence levels of up to 50 mJ/cm^2 were used. Again, no enhancements in the photorefractive effects were observed.

V. OTHER SECONDARY CENTER EFFECTS

In the course of this effort it became apparent that the secondary photorefractive centers were responsible for many photorefractive characteristics of $BaTiO_3$ which are not explained by the usual model for photorefraction. Two of these effects are the sublinear intensity dependence of the grating formation time constant and the temperature-dependent two beam coupling effective trap concentration.

Sublinear intensity dependence

An important issue in the application of the photorefractive effect is the speed of the grating formation. According to the widely used results of Kukhtarev[2], the grating formation time is expected to be inversely proportional to the laser intensity. However, experiments performed on barium titanate have shown that the response time varies with intensity as I^{-x}, where the exponent x ranges from 0.5 to 1.0.[4-6] In this section we show that this sublinear dependence of the photorefractive grating formation time is explained by the presence of secondary photorefractive centers. For convenience, the derivation is limited to the presence of only one type of secondary center.

According to the Kukhtarev solutions, the photorefractive response time τ can be written as[7].

$$\tau = \tau_{die} \frac{1 + K^2 L_D^2}{1 + K^2 L_S^2}, \tag{18}$$

where τ_{die} is the dielectric relaxation time given by

$$\tau_{die} = \epsilon\epsilon_o / q\mu_h N_{h0}, \tag{19}$$

L_S and L_D are the screening and diffusion lengths, respectively, given by

$$L_S^2 = \epsilon\epsilon_o k_B T / q^2 N_E \tag{20}$$

and

$$L_D^2 = \mu_h k_B T \tau_h / q, \tag{21}$$

K is the grating wave number, N_E is the effective empty trap density, μ_h is the hole mobility, N_{h0} is the mean free carrier

concentration, τ_h is the free carrier lifetime, ϵ is the dielectric constant. In the single donor-trap model, N_{h0} is the only intensity-dependent parameter which affects equation (18). It is simply proportional to the laser intensity, and consequently, the response time is expected to vary inversely with intensity.

The important feature of the secondary center model is the finite thermal ionization rate of the secondary centers ($\beta_2 \approx 30$ sec^{-1}) which influences the free carrier and occupied trap concentrations. The photorefractive response time predicted by the secondary center model can be determined in a manner similar to that used by Valley[8]. We start with the equations used to calculate the steady-state space-charge field:

$$dN_1/dt = -(S_{11}I_1 + \beta_1)N_1 + \gamma_1(N_{1T} - N_1)N_h \quad (22)$$

$$dN_2/dt = -(S_{21}I_1 + S_{22}I_2 + \beta_2)N_2 + \gamma_2(N_{2T} - N_2)N_h \quad (23)$$

$$dN_h/dt = -dN_1/dt - dN_2/dt \quad (24)$$

$$\partial N_h/dt = dN_h/dt - \nabla\cdot j_h \quad (25)$$

$$j_h = \mu_h N_h E - D\nabla N_h, \quad (26)$$

$$\nabla\cdot E = \rho/\epsilon\epsilon_o, \quad (27)$$

Solution of equations (22 -27) proceeds by setting N_1, N_2, N_h, and E to the form $X = X_0 + X_1$ and solving for the lowest Fourier component in the quasi-steady approximation[1]. The X_0 quantities are assumed to be independent of space and time while the first order quantities are assumed to be of the form $\exp(iKz-\Gamma t)$. This yields the following set of simultaneous equations in the first order variables:

$$(\Gamma_1-\Gamma)N_{11} - \Gamma_{R1}n_{h1} = -S_1I_0mN_{10} \quad (28)$$

$$(\Gamma_2-\Gamma)N_{21} - \Gamma_{R2}N_{h1} = -S_2I_0mN_{20} \quad (29)$$

$$\mu_hN_{h0}A_1 - \Gamma N_{11} - \Gamma N_{21} + (\Gamma_D-\Gamma)N_{h1} = 0 \quad (30)$$

$$(-\epsilon\epsilon_0/q)A_1 + N_{11} + N_{21} + N_{h1} = 0 \quad (31)$$

where $\Gamma_1 = S_1I_0+\beta_1+ {}_1N_{h0}$, $\Gamma_2 = S_2I_0+\beta_2+ {}_2N_{h0}$, $\Gamma_{R1} = {}_1(N_{1T}-N_{10})$, $\Gamma_{R2} = {}_2(N_{2T}-N_{20})$, $\Gamma_D = K^2\mu_hk_BT/q$, and $\Gamma_{die}= \mu_hN_{h0}q/\epsilon\epsilon_o$, m is the intensity modulation index, $A_1 = iKE_1$, and $E_0=0$. N_{10}, N_{20}, and N_{h0} are constants determined from the zeroth order equations. The photorefractive response time $1/\Gamma$ is found by setting the determinant of left hand side of equations (28-31) equal to zero. With the approximation $\Gamma_D >> \Gamma_{die}-\Gamma$, this yields equation for the photorefractive response time $1/\Gamma$

$$(\Gamma_D+\Gamma_{R2}+\Gamma_{R1})\Gamma^2 - [\ \Gamma_D(\Gamma_1+\Gamma_2) + \Gamma_{die}(\Gamma_{R1}+\Gamma_{R2}) + \Gamma_1\Gamma_{R1} + \Gamma_2\Gamma_{R1}\ ]\Gamma + [\Gamma_D\Gamma_1\Gamma_2 + \Gamma_{die}\Gamma_1\Gamma_{R2} + \Gamma_{die}\Gamma_2\Gamma_{R1}] = 0. \quad (32)$$

The intensity dependence of the response time is shown in Figure 14. The lines are theoretical results calculated from equation (32) and the circles and triangles are experimental data. This data was taken on an as-grown p-type barium titanate crystal using the 514.5 nm line of an argon-ion laser. The grating wavevector was parallel to the C-axis and the light had ordinary polarization. The ratio of the signal beam to the pump beam was 0.03 to 1. We monitored the change in power of the signal beam in the presence of the pump beam and found the time dependence of the grating formation to be described as a single exponential. The power law dependencies determined from a fit

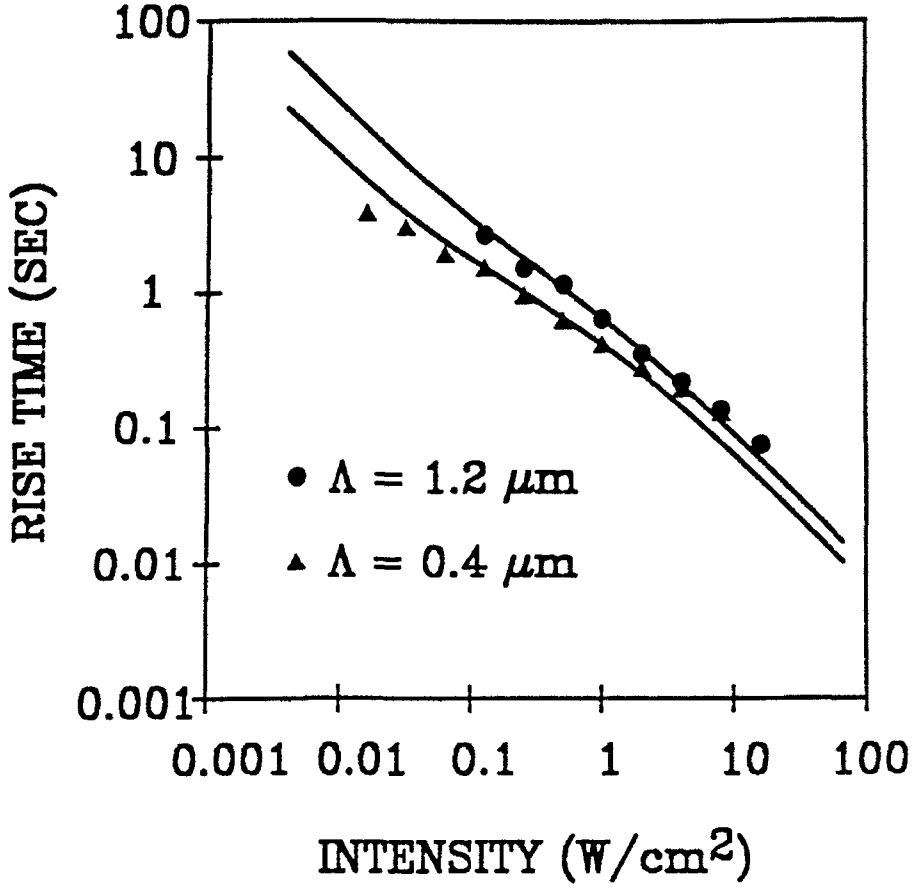

Figure 14. Photorefractive rise time versus incident laser intensity for 0.4 and 1.2 μm grating periods. The circles and triangles are experimental data and the lines are secondary-center model theory.

the data to an I^{-x} form were $I^{-0.73}$ for a 1.2 μm grating period and $I^{-0.56}$ for a 0.40 μm grating period. The parameter values used in the calculations are listed below and are the same that were used in reference 1 to model the steady-state characteristics of the same barium titanate crystal. The hole mobility was the only new parameter. Changing the magnitude of the mobility did not change the shape of the curve, but did determine the magnitude of the response time. We found that a value of about 0.25 cm^2/V-sec best matched the magnitude of the experimental response times.

The theoretical curves were only approximately of the form I^{-x}. The response times varied as 1/I at the low and high intensity regimes but were sublinear at intermediate intensities, the region of most experiments. A fit of the theoretical curves to an I^{-x} functional form over an intensity range of 0.01 to 10.0 W/cm^2 gave power law dependencies of $I^{-0.78}$ and $I^{-0.69}$ for the 1.2 and 0.4 μm grating periods, respectively.

It is convenient to discuss the effect of the secondary centers on the response time by using equation (18). This expression remains meaningful for the secondary center model; it is the values of the dielectric relaxation time and diffusion and screening length which are model dependent. The same results were obtained using either equations (18) or (32).

The free carrier concentration influences the photorefractive response time through the $1/N_{h0}$ dependence of the dielectric relaxation time. One important consequence of the secondary center model is the sublinear dependence of the free carrier concentration on laser intensity. This is shown in Fig. 15. Here

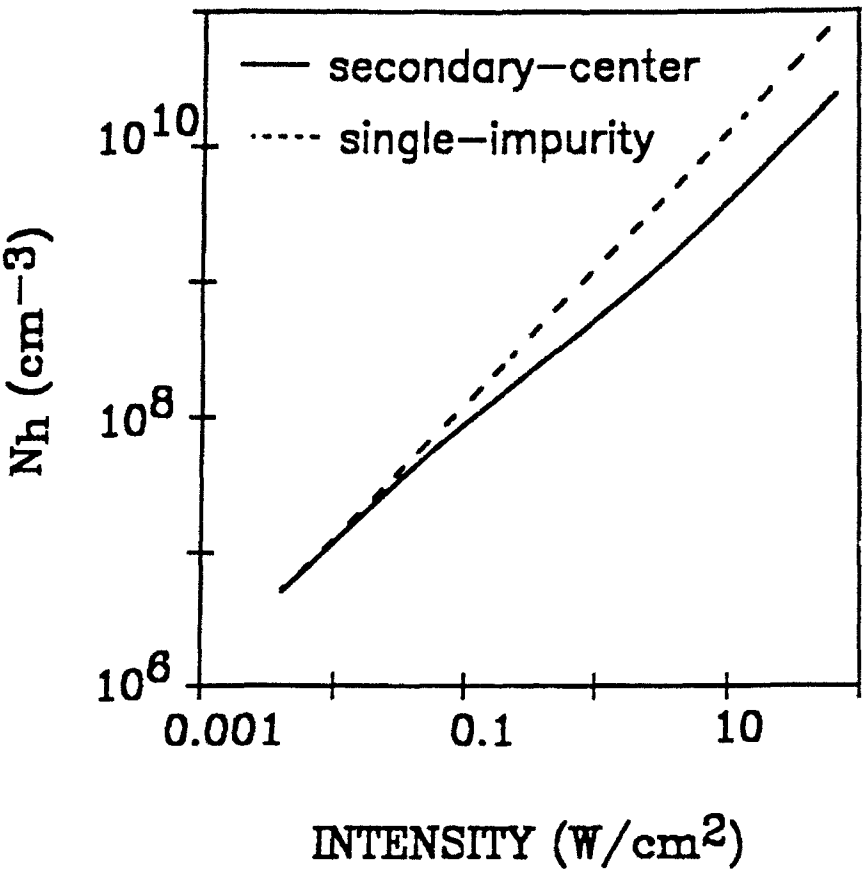

Figure 15. Free carrier concentration versus laser intensity for the secondary-center and single-impurity models.

we plot the calculated steady-state free carrier concentration under uniform illumination as a function of laser intensity for both the single-impurity and the secondary-center models. While the free carrier concentration increases linearly with intensity for the single-impurity model, the presence of secondary centers results in a sublinear dependence.

The response time also depends on the screening and diffusion lengths, as seen by examination of equation (18). From this equation we see that at long grating periods (> 4.0 μm in $BaTiO_3$) the response time is approximately equal to the dielectric relaxation time. At smaller grating periods the second term is significant. In $BaTiO_3$ the screening length is typically larger than the diffusion length and, therefore, the response time decreases as the grating period decreases.

The diffusion length may vary as a result of an intensity dependence in the free carrier lifetime, due to changes in the occupied trap concentrations. This is shown in Fig. 16 where we plot the lifetime versus intensity. A more important effect is the intensity dependence of the screening length. According to equation (20), L_s^2 is inversely proportional to N_E. As was shown in reference 1, the effective empty trap concentration increased with laser intensity due to the contribution of the secondary centers to the redistribution of charges. This effect is shown in Fig. 16 where we plot N_E versus laser intensity. The effective empty trap concentration increased by about a factor of 5 between intensities of 0.1 and 10 W/cm^2.

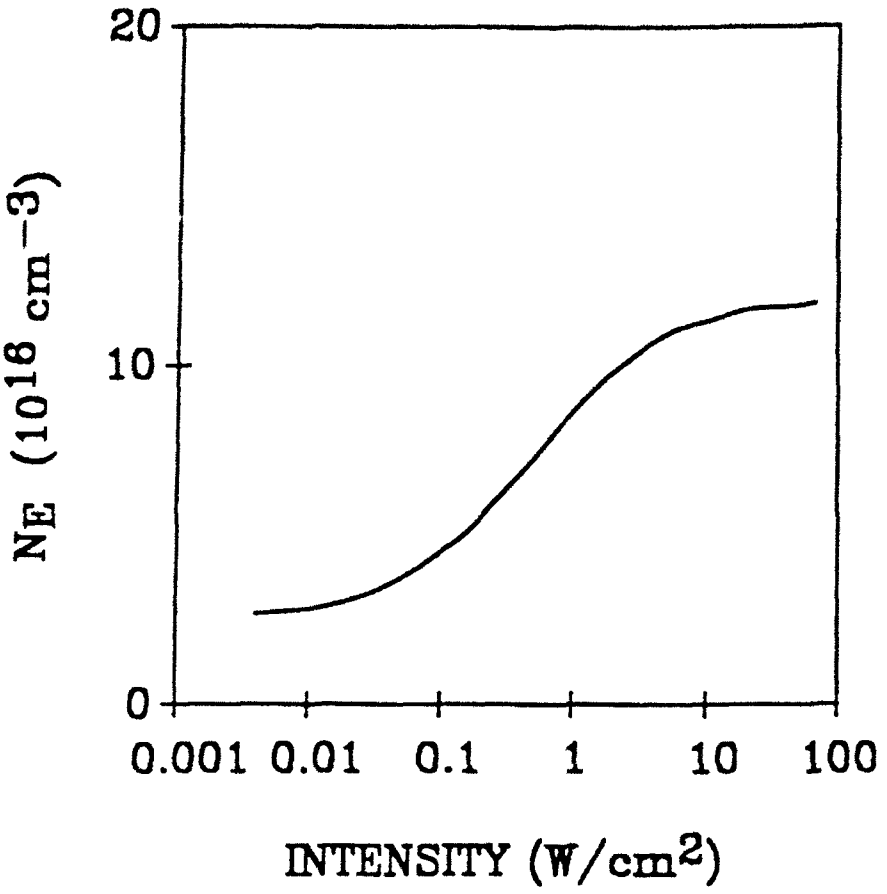

Figure 16. Effective empty trap concentration and free carrier lifetime versus laser intensity for the secondary center model.

In Figure 17 we plot the calculated power law dependence of the photorefractive rise time versus intensity as a function of grating period. This was determined by fitting the theoretical curves to an I^{-x} functional form for intensities between 0.01 and 10 W/cm^2. At long grating periods the power law dependence is the same as that of the dielectric relaxation time and is determined by the sublinear free carrier dependence, as shown in Fig 15. At small grating periods the exponent decreases with decreasing grating period. This is a result of the intensity-dependence of the characteristic lengths, primarily that of the screening length due to the intensity-dependent effective empty trap concentration.

Parameter values used in the above calculations are: $S_1 = 2.5X10^{-19}$ cm^2, $S_2 = 5X10^{-18}$ cm^2, $_1 = 5X10^{-8}$ cm^3s^{-1}, $_2 = 2.5X10^{-8}$ cm^3sec^{-1}, $\beta_1 = 1.5X10^{-4}$ sec^{-1}, $\beta_2 = 30$ sec^{-1}, $N_{1T} = 2.6X10^{18}cm^{-3}$, $N_1(0) = 2.57X10^{18}$ cm^{-3}, $N_{2T} = 1.5X10^{17}$ cm^{-3}, $N_2(0) = 3.8X10^{13}$ cm^{-3}, $N_h(0) = 3X10^5$ cm^{-3}, $\epsilon = 168$, and $\mu_h = 0.25$ $cm^2V^{-1}s^{-1}$.

Temperature dependent photorefractive effects

In 1988 Rytz *et al.*[9] reported results of two-wave mixing experiments performed on $BaTiO_3$ crystals in the temperature range between 20° and 120°C. They observed a large decrease in the density of empty traps as well as a significant decrease in the response time at elevated temperatures. These characteristics are not in agreement with the usual band transport model of

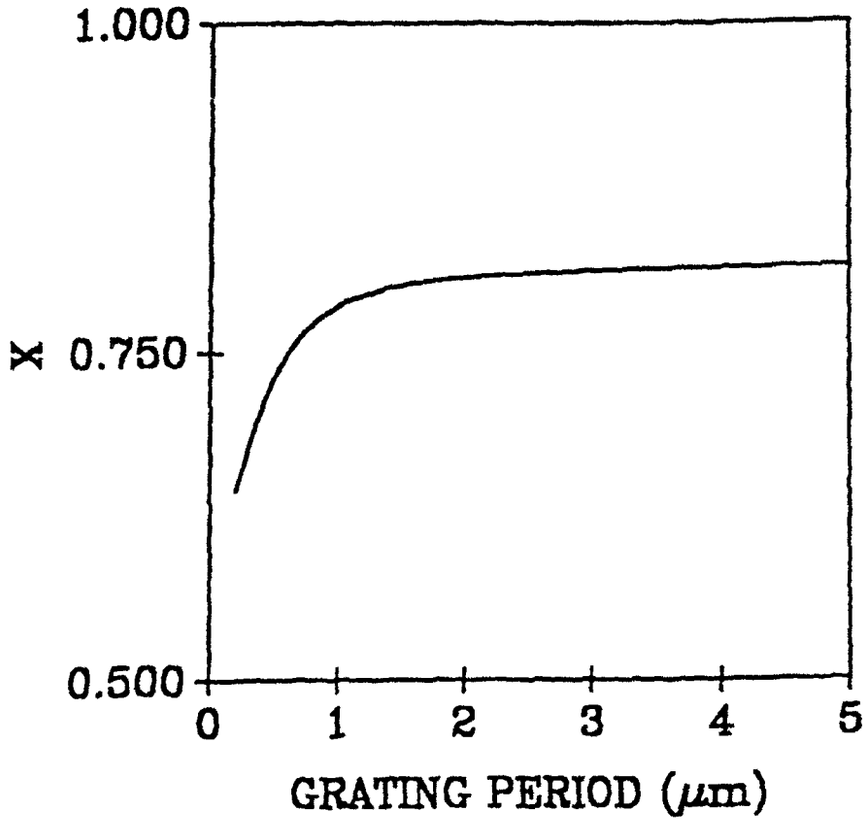

Figure 17. Calculated power law dependence of the photorefractive rise time versus laser intensity as a function of grating period. The exponent x was calculated according to $\tau = AI^{-x}$.

photorefraction. In Figure 18 we show some of the experimental results obtained by Rytz *et al.*[9]. In Figure 19 we plot the behavior expected from the standard "Kukhtarev" model. The physical mechanism for the observed differences was not well understood.

These temperature dependent photorefractive effects can be explained by secondary centers. At the intensities of 2 to3 W/cm^2 used by Rytz *et al.*[9] these centers are easily populated. To demonstrate the effect of secondary centers the temperature dependence of the two-wave mixing gain was calculated based on the secondary center model. For these calculations a model of one species of secondary centers with a thermal activation energy of 0.5 eV was used. Values for the dielectric constant at different temperatures were taken from reference 10. The electro-optic coefficient was assumed to be proportional to the dielectric constant and temperature variations in the refractive index were neglected.

The calculated variations in the two-wave mixing gain coefficient with temperature are shown in Figure 20. These predictions are very similar to the experimental results of Rytz *et al.*[9], and are consistent with a decrease in the effective empty trap concentration with an increase in temperature. This is also consistent with the observed decrease in magnitude of the photo-induced absorption with increasing absorption.

Rytz *et al.*[9] also found that the photorefractive response time decreased significantly with temperature increase. the magnitude of this effect is not predicted by the secondary center model if it is assumed that the hole mobility is constant.

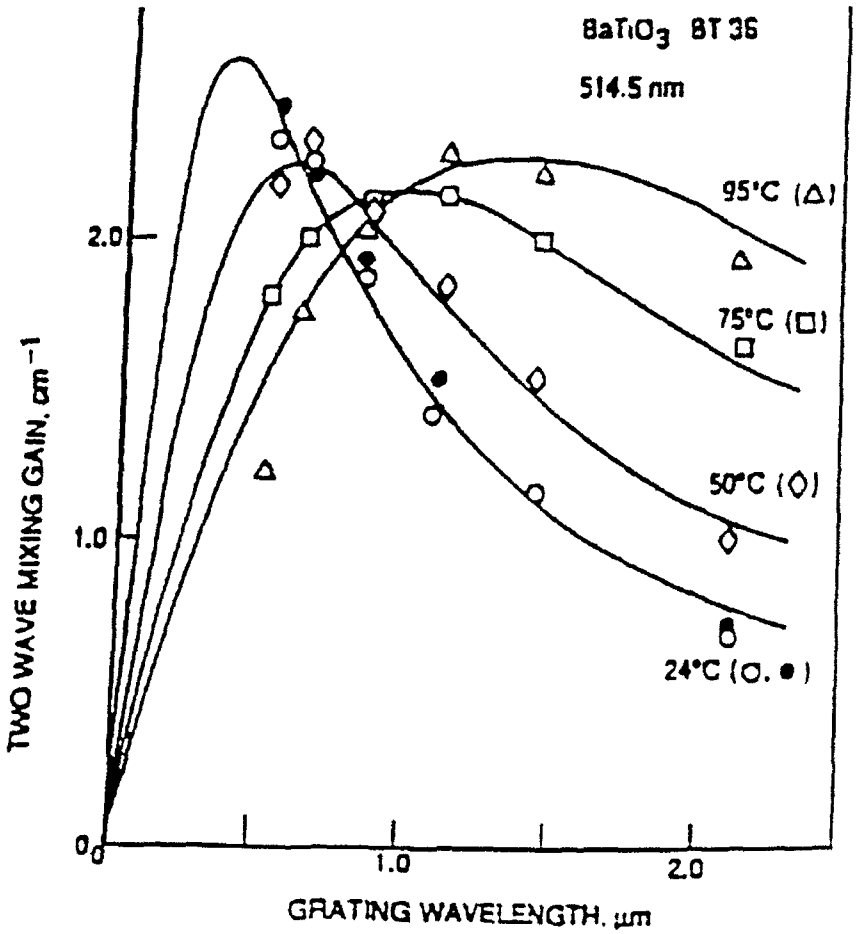

Figure 18. Experimental two-wave mixing gain vs grating period for different temperatures reported in reference 9.

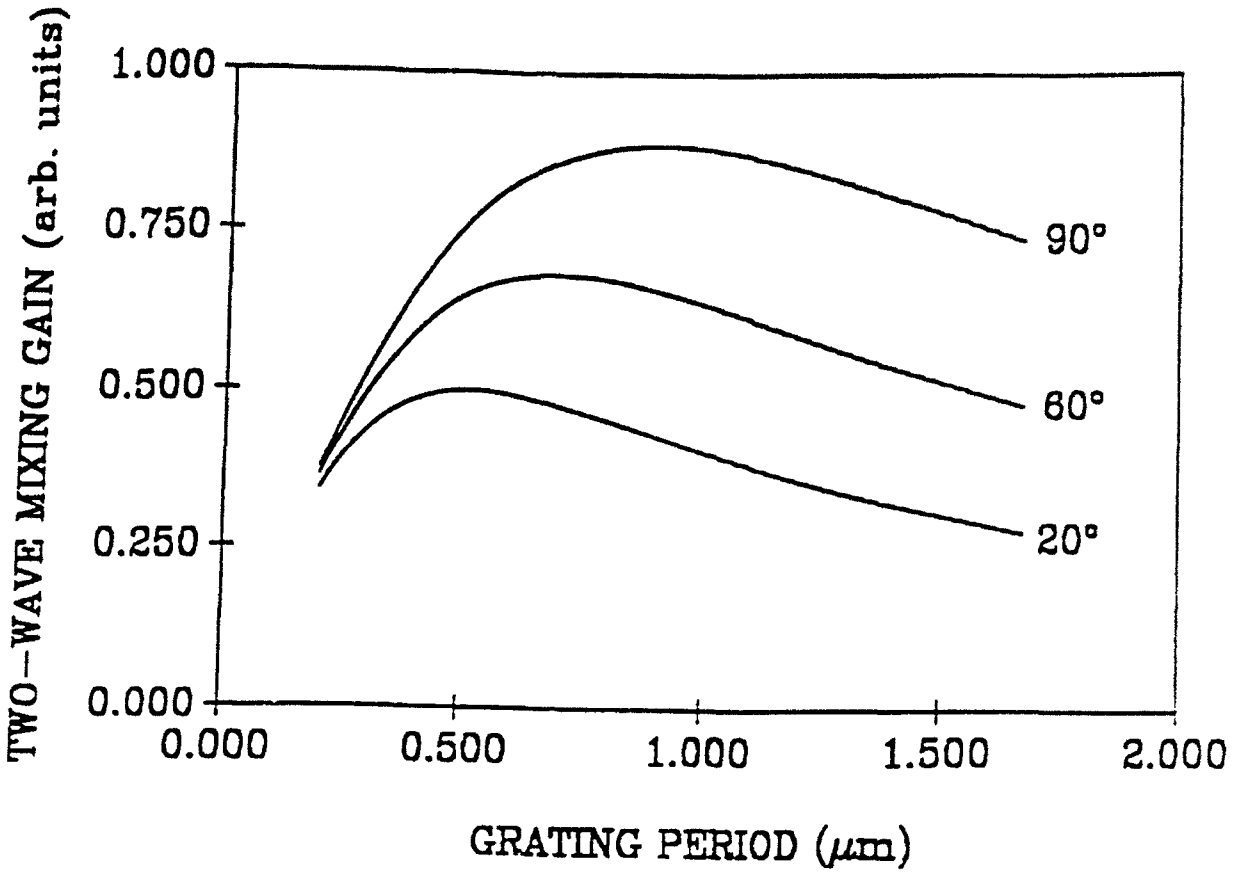

Figure 19. Calculated two-wave mixing gain vs grating period for different temperatures for standard single species "Kuhktrarev" model.

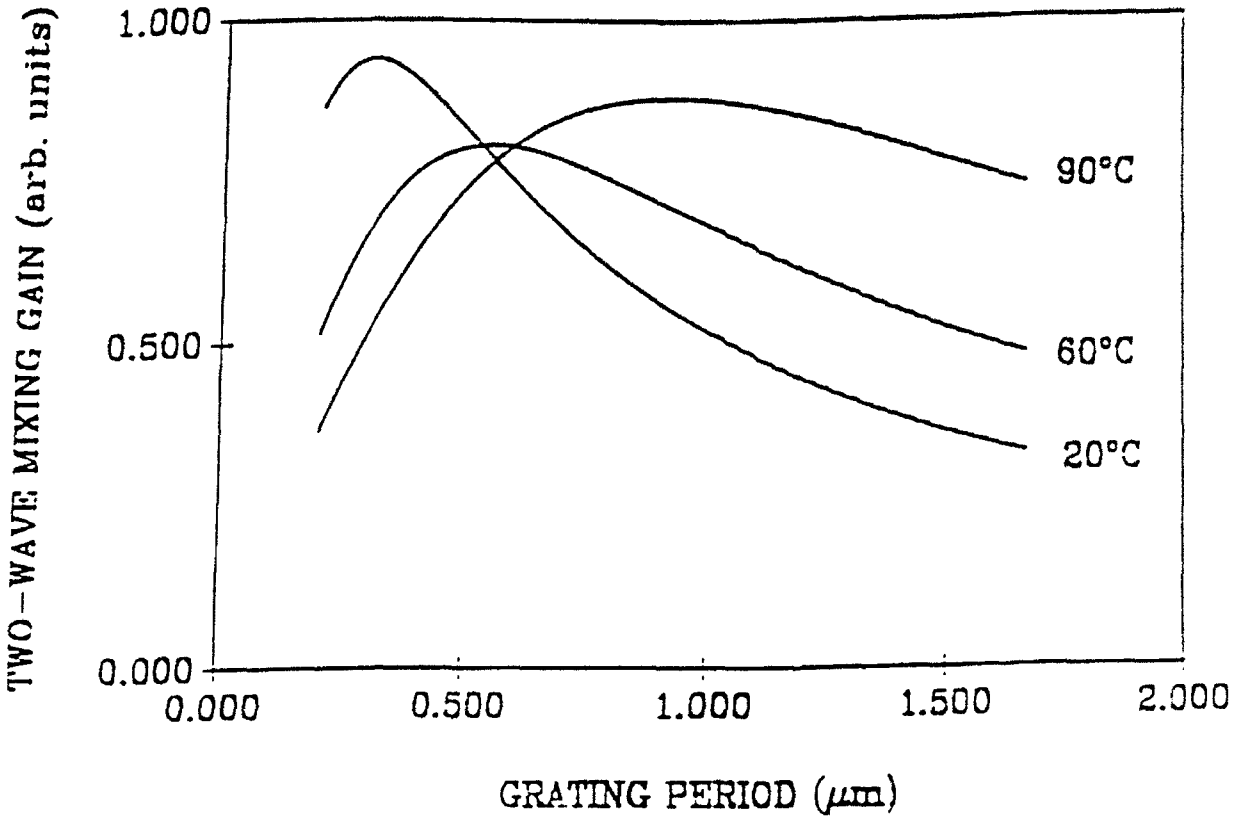

Figure 20. Calculated two-wave mixing gain vs grating period and temperature for incident intensity of 3 W/cm^2.

Agreement with experimental results requires a hole mobility which increases with temperature with an activation energy similar to the thermal ionization energy of the secondary centers, characteristic of a trap dominated mobility. This suggests that the secondary centers exhibit a strong influence on the hole mobility and therefore photorefractive response time in $BaTiO_3$.

VI. SUMMARY

In this effort the effects of secondary centers on the photorefractive properties of $BaTiO_3$ were investigated with the goal of obtaining enhancements in the photorefractive effects through utilization of the secondary centers by external pumping. Secondary center parameters were measured through photo-induced absorption and two-beam coupling experiments. These experiments demonstrated that two species of secondary centers (denoted by N_2 and N_3) were present, with concentrations of approximately 1.5×10^{17} cm^{-3} and 2×10^{16} cm^{-3}. It was discovered that at near IR wavelengths ($\approx$ 800 nm) these secondary centers were already being populated and thus contributing to and enhancing the photorefractive effect. Consequently, enhancement of the photorefractive effect through external pumping was not realized.

A numerical method, based on a finite difference approach, was developed to model the secondary center effects. Although the computation time required to implement the calculations was prohibitive, this numerical capability has been successfully

utilized to calculate photorefractive grating formations in other crystals such as $Bi_{12}SiO_{20}$ in which the calculations are less computationly intensive.

VII. REFERENCES

1. G.A. Brost, R.A. Motes, and J.R. Rotge', J. Opt. Soc. Am B. **5**, 1879 (1988)
2. N.V. Kukhtarev, Sov. Tech. Phys. Lett. **2**, 438 (1976).
3. R.A. Motes and J.J. Kim, J. Opt. Soc. Am B **4**, 1379 (1987).
4. S. Ducharme and J. Feinberg, J. Appl. Phys. **56**, 839 (1984).
5. R.L. Townsend and J.T. LaMacchia, J. Appl. Phys. **41**, 5188 (1970).
6. D. Rak, I. Ledoux, and J.P. Huignard, Opt. Commun. **49**, 302 (1984).
7. G.C. Valley and J.F. Lam in "Photorefractive Materials and Their Applications I", P. Gunter and J.-P. Huignard, eds. (Springer Verlag, Berlin, 1988)
8. G.C. Valley, J. Appl. Phys. **59**, 3363 (1986).
9. D. Rytz, M.B., Klein, R.A. Mullen, R.N. Schwartz, G.C. Valley, and B.A. Wechsler, Appl. Phys. Lett. **52**, 1759 (1988).
10. S.H. Wemple, M. DiDomenico, and I. Camlibel, J. Phys. Chem. Solids **31**, 1417 (1970).

*U.S. GOVERNMENT PRINTING OFFICE 1993-

MISSION

OF

ROME LABORATORY

Rome Laboratory plans and executes an interdisciplinary program in research, development, test, and technology transition in support of Air Force Command, Control, Communications and Intelligence (C^3I) activities for all Air Force platforms. It also executes selected acquisition programs in several areas of expertise. Technical and engineering support within areas of competence is provided to ESD Program Offices (POs) and other ESD elements to perform effective acquisition of C^3I systems. In addition, Rome Laboratory's technology supports other AFSC Product Divisions, the Air Force user community, and other DOD and non-DOD agencies. Rome Laboratory maintains technical competence and research programs in areas including, but not limited to, communications, command and control, battle management, intelligence information processing, computational sciences and software producibility, wide area surveillance/sensors, signal processing, solid state sciences, photonics, electromagnetic technology, superconductivity, and electronic reliability/maintainability and testability.